China Geology 7 (2024) 91−103

China Geology

Journal homepage: http://chinageology.cgs.cn
https://www.sciencedirect.com/journal/china-geology

An integrated north–south paleo-Dadu-Anning River: New insights from bulk major and trace element analyses of the Xigeda Formation

Yong Zheng[a, b, c,*], Hai-bing Li[a, b, c], Jia-wei Pan[a, b, c], Ping Wang[d], Ya Lai[a, b, c], Zheng Gong[e]

[a] *Key Laboratory of Deep-Earth Dynamics*, *Institute of Geology*, *Chinese Academy of Geological Sciences*, *China Geological Survey*, *Ministry of Natural Resources*, *Beijing* 100037, *China*
[b] *Jiangsu Donghai Continental Deep Hole Crustal Activity National Observaion and Research Station*, *Lianyungang* 222300, *China*
[c] *Southern Marine Science and Engineering Guangdong Laboratory*, *Guangzhou* 511458, *China*
[d] *Geophysical Exploration Center*, *China Earthquake Administration*, *Zhengzhou* 450002, *China*
[e] *Institute of Geophysics*, *China Earthquake Administration*, *Beijing* 100081, *China*

ARTICLE INFO

Article history:
Received 12 October 2022
Received in revised form 7 February 2023
Accepted 15 March 2023
Available online 24 April 2023

Keywords:
Dadu River
Anninghe fault
River diversion
Xigeda Formation
Tectonic uplift
Provenance
Songpan-Ganzi flysch
Ancient lake
Xianshuihe-Xiaojiang fault system
Tibetan Plateau

ABSTRACT

The Xianshuihe-Anninghe fault extends SE–S and constitutes the southeastern margin of the Tibetan Plateau. However, the Dadu River which is associated with the fault does not flow following the path, but makes a 90º turn within a distance of 1 km at Shimian, heading east, and joins the Yangtze River, finally flowing into the East China Sea. Adjacent to the abrupt turn, a low and wide pass near the Daqiao reservoir at Mianning separates the N–S course of the Dadu River from the headwater of the Anning River which then flows south into the Yunnan Province along the Anninghe fault. Therefore, many previous studies assumed southward flow of the paleo-Dadu River from the Shimian to the Anning River. However, evidences for the capture of the integrated N–S paleo-Dadu-Anning River, its timing, and causes are still insufficient. This study explored the paleo-drainage pattern of the Dadu and Anning Rivers based on bulk mineral and geochemical analyses of the large quantities of fluvial/lacustrine sediments along the trunk of the Dadu and Anning Rivers. Similar with sands in the modern Dadu River, the Xigeda sediments also exhibit a granitoid affinity with the bulk major mineral compositions of quartz (>50%), anorthite (about 10%), orthoclase (about 5%), muscovite (about 5%), and clinochlore (about 4%). Correspondingly, bulk major elements show high SiO_2, with all samples >60%, and some of them >70%, low TiO_2 (⩽0.75%), P_2O_5 (⩽0.55%), FeO* (⩽5%), and relatively high CaO (1.02%–8.51%), Na_2O (1.60%–2.52%), and K_2O (2.17%–2.71%), with a uniform REE patterns. Therefore, synthesizing all these results indicate that these lacustrine sediments have similar material sources, which are mainly derived from its course in the Songpan-Ganzi flysch block, implying that the paleo-Dadu originally flowed southward into the Anning River and provided materials to the Xigeda ancient lake. The rearrangement of the paleo-Dadu River appears to be closely related to the locally focused uplift driven by strong activities of the Xianshuihe-Xiaojiang fault system.

1. Introduction

Different from other margins of the Tibetan Plateau, the southeastern Tibet is characterized by uniquely low and continuous gradient, 5 km elevation gain over 1500 km in length (Fig. 1a). Several thousand-kilometer scale rivers which are originating from the Qinghai-Tibetan Plateau, traverse across the low-relief surface, from west to east, namely, the Salween River, the Mekong River, the Yangtze River, the Yalong River, and the Dadu River. The Xianshuihe-Anninghe fault extents SE–S and constitutes the southeastern margin of the Tibetan Plateau. However, the Dadu River which is associated with the fault does not flow following its path. It originates from the Songpan-Ganzi terrane separated from the upstream part of the Yellow River by the Bayan Har Mountains, first flows south along its upper course, and then this river abruptly flows east (Fig. 1b), forming a about 90º bend within a distance of one km at Shimian. From here, it is separated from the headwaters of the about N–S Anning River by a low, wide pass near the Daqiao reservoir at Mianning. Therefore, the occurrence of river

* Corresponding author: *E-mail address*: zygeology@163.com (Yong Zheng).

Literary editor: Xi-jie Chen
doi:10.31035/cg2023027
2096-5192/© 2024 China Geology Editorial Office.

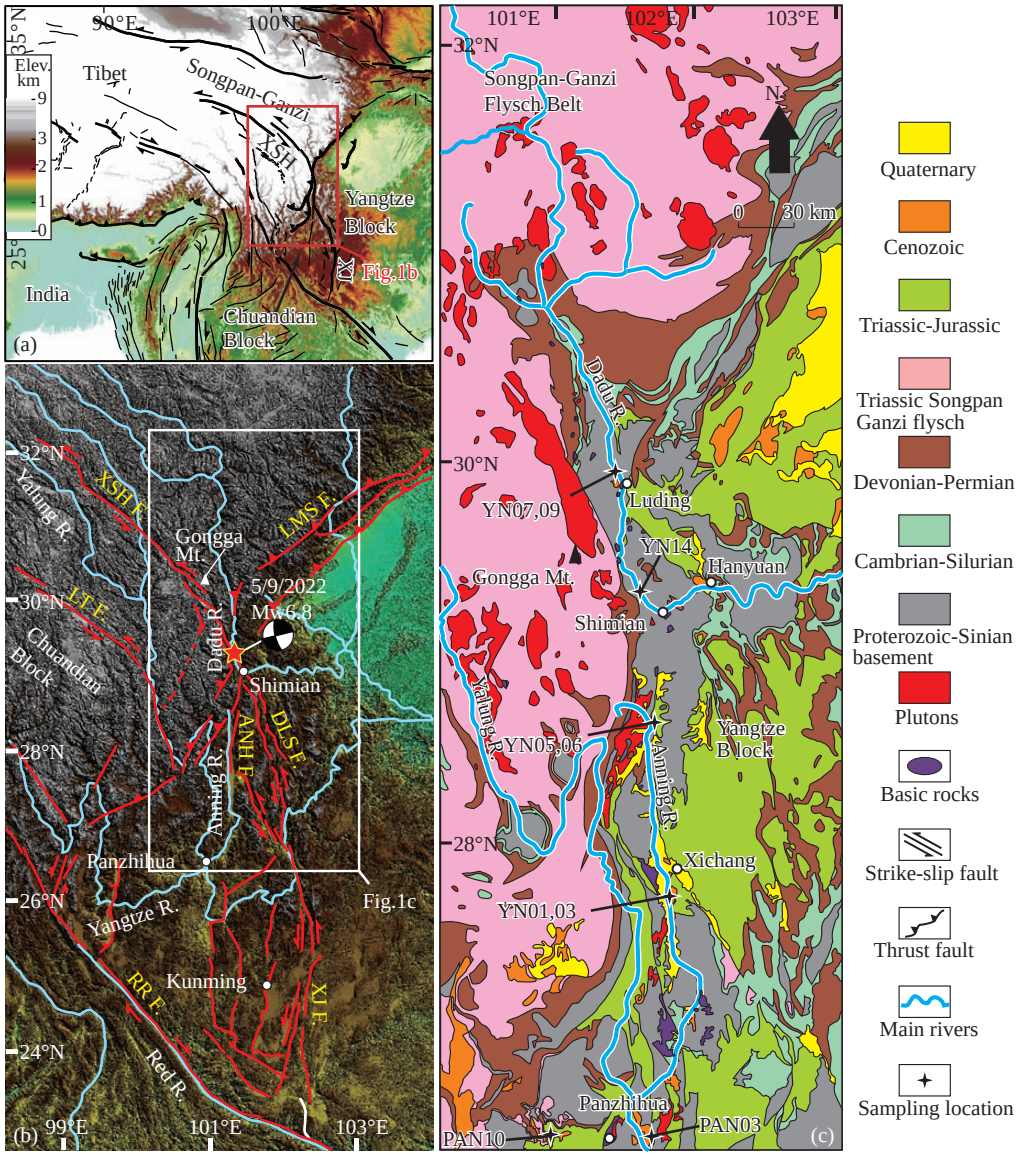

Fig. 1. Tectonic and geological setting of southeastern Tibet. a–Tectonic sketch of SE Asia; b–topography, major rivers and active faults in southeastern Tibet; c–geological map showing the main catchment of the Dadu River and Anning River, and the sampling locations of this study.

capture between Shimian and Mianning assuming southward flow of the paleo-Dadu River from the Shimian to the Anning River has been suggested (Deng B et al., 2020; Yang R et al., 2020). However, the timing and events responsible for the capture of the Dadu River are still debated, and there are few constraints on when the capture occurred resulting in the current drainage system (Zheng Y et al., 2023).

Clark MK et al. (2004) first suggested that the paleo-Dadu originally drained into the Anning River, then joined in the Yangtze River at Panzhihua. Drainage reorganization occurs for several reasons: tectonic movement, natural damming and erosion. Indeed, hundreds of meters thick lacustrine sediments are found along the Dadu and Anning Rivers, which are described as Xigeda layer in the Chinese literature, and their formation is regarded as the only direct record of the drainage rearrangement response to local tectonic activities. However, up to date, except detrital zircon U-Pb dating (Yang R et al., 2020; Zhao XD et al., 2021; Zheng Y et al., 2023), no other evidences have been reported to support the idea that the paleo-Dadu River once integrated with the Anning River and then was captured owing to local uplift. Therefore, whether an integrated paleo-Dadu-Anning River ever existed or not is still doubted.

Geochemical composition of sedimentary rocks provides a record of their tectonic setting and provenance (Taylor SR and Mclennan SM, 1985; Bhatia MR and Crook KAW, 1986; Gu XX et al., 2002), which is probably among the few useful avenues to evaluate the development of fluvial systems associated with tectonic activities. In this study, we analyzed bulk mineral compositions, major and trace elements to discuss the provenance of the Xigeda Formation along the Dadu and Anning Rivers. Based on these data, we provide more evidences for the once occurrence of an integrated paleo-Dadu-Anning River and explore their implications in regional neotectonic movement in southeastern Tibet.

2. Geological setting

The Dadu River and Anning River in southeastern margin of Tibet are the major tributaries of the Yangtze River, which not only provide abundant erosional debris, but also sculpted the low-relief, high-elevation topography (Figs. 1a, b). Their drainage area mainly consists of two geological units (Fig. 1c). The western unit is constituted by the Songpan-Ganzi flysch belt which was developed from a large foreland basin during the Triassic orogeny (Xu ZQ, 1992). Its main sedimentary cover is constituted by the flysch belt which is mainly composed of deep-marine siliciclastic turbidite (Xu ZQ, 1992) and was widely emplaced by granitoid magma during Middle Triassic-Early Jurassic (Roger F et al., 2004). The Neoproterozoic flysch, sodic volcanic rocks, and carbonates constitute the eastern unit, belonging to the Yangtze Block (Li ZX et al., 2003). The sedimentary cover is thin with weak magmatism and varies from the clastic rocks, carbonates, basic volcanic rocks, and coal-bearing layers of the marine-terrigenous environment of the Sinian-Late Triassic to the continental sedimentation dominated by the coal-bearing molasse and red clastic rocks during the Late Triassic-Cenozoic.

The Xianshuihe-Xiaojiang fault system is the major structure (Fig. 1b) and is characterized by the most strike-slip faulting and frequent earthquake activities (Bai MK et al., 2018). From north to south, the Xianshuihe-Xiaojiang fault system can be divided into four segments: Ganzi-Yushu, Xianhuihe, Anninghe-Daliangshan and Xiaojiang faults. The Xianshuihe fault turns from NW–SE into about N–S near Shimian and splits into two left-lateral strike-slip branches: the Anninghe fault and the Daliangshan fault (Fig. 1b). As a result, an abut between the Xianshuihe fault and Anninghe-Daliangshan fault occurs coincidently with the remarkable about 90º turn of the Dadu River (Fig. 1b). The *M* w 6.8 Luding earthquake occurred exactly within this transition zone on September 5, 2022. Then, the Anninghe fault guides the southward flowing of the Anning River.

Along the Dadu River, the Xigeda lacustrine sediments only occur upstream of Luding at 1800–2200 m, and downstream of Shimian at Hanyuan with elevations of 900–1100 m. These sediments mainly consist of interbedded unconsolidated fine-grained sands, silts, and silty clays (Fig. 2a), with different elevations. Conglomerates lie unconformably beneath the lacustrine sediments in Luding and fluvial cobbles and sands are preserved overlying them as high terraces over the Dadu River. In the Mianning County along the Anning River, the sediments occur with an approximately 300 m thickness and a top elevation of 1972 m. This section shows a gray color in general and mainly consists of medium-fine sand layers with interbedded silty clays (Fig. 2b). The sediments are unconformably overlying on the Pre-Sinian metamorphic rocks. Southward around the Qionghai Lake near Xichang, most sediments occur at elevations between 1600 m and 1650 m, with thicknesses ranging from 140 m to 200 m. The sediments are mainly composed of silt and clay layers with

Fig. 2. Collected fluvial/lacustrine sand samples in the (a) Luding, (b) Mianning, (c) Xichang and (d) Panzhihua sections.

development of horizontal laminations (Fig. 2c). The Xigeda layers occur continuously between heights of 970 m and 1500 m at Panzhihua (Fig. 2d), downstream of the Anning River.

3. Sampling and methodology

Along the spiral cut, we have collected two lacustrine samples from the Luding section (YN07 and YN09), and a sand sample (YN14) from the lowest terrace of the Dadu River (Fig. 1c). Based on cosmogenic nuclide burial dating, the Luding sediments were deposited at about 1.2 Ma ago owing to paleo-landslide associated with the strike-slip faulting of the Xianshuihe fault (Zheng Y et al., 2023). Along the Anning River, we collected two samples from the Mianning section (YN05 and YN06) along an incised terrace. Two samples from the Xichang section (YN01 and YN03) were collected at the base of a construction slope. From the Panzhihua section, We collected one sample (PAN10) along the road through the Xigeda villiage, and one sample (PAN03) from a playground construction slope. The deposition ages of these sediments are about 0.6 Ma ago, about 0.9 Ma ago and about 1.2 Ma ago, respectively (Kong P et al., 2009; Zheng Y et al., 2023), and the deposition is attributed to the subsidence of the Anning graben. The sampling depths are shown as Fig. 3. All samples are located at siltstone layers interbedded with clay layers (Fig. 2), thus are characterized by lacustrine sediments with grain size <63 μm. Synthesizing these data, we traced the provenance and origin of the Xigeda sediments and discussed reorganization of the paleo-Dadu-Anning River.

The bulk mineral compositions of the samples were analyzed using powder X-ray diffraction (XRD) at Institute of Geology, Chinese Academy of Sciences (IGGCAS). The randomly mounted samples were scanned from 3º–65º (2θ) using a DMAX 2400 diffractometer (CuKα) at 40 kV and 60 mA, with a scanning speed of 4 deg/min and a sampling width of 0.02º.

The bulk major element oxides were analyzed using a Shimadzu1500 X-ray fluorescence spectrometer with analytical precisions ranging from 1% to 5%, and the bulk

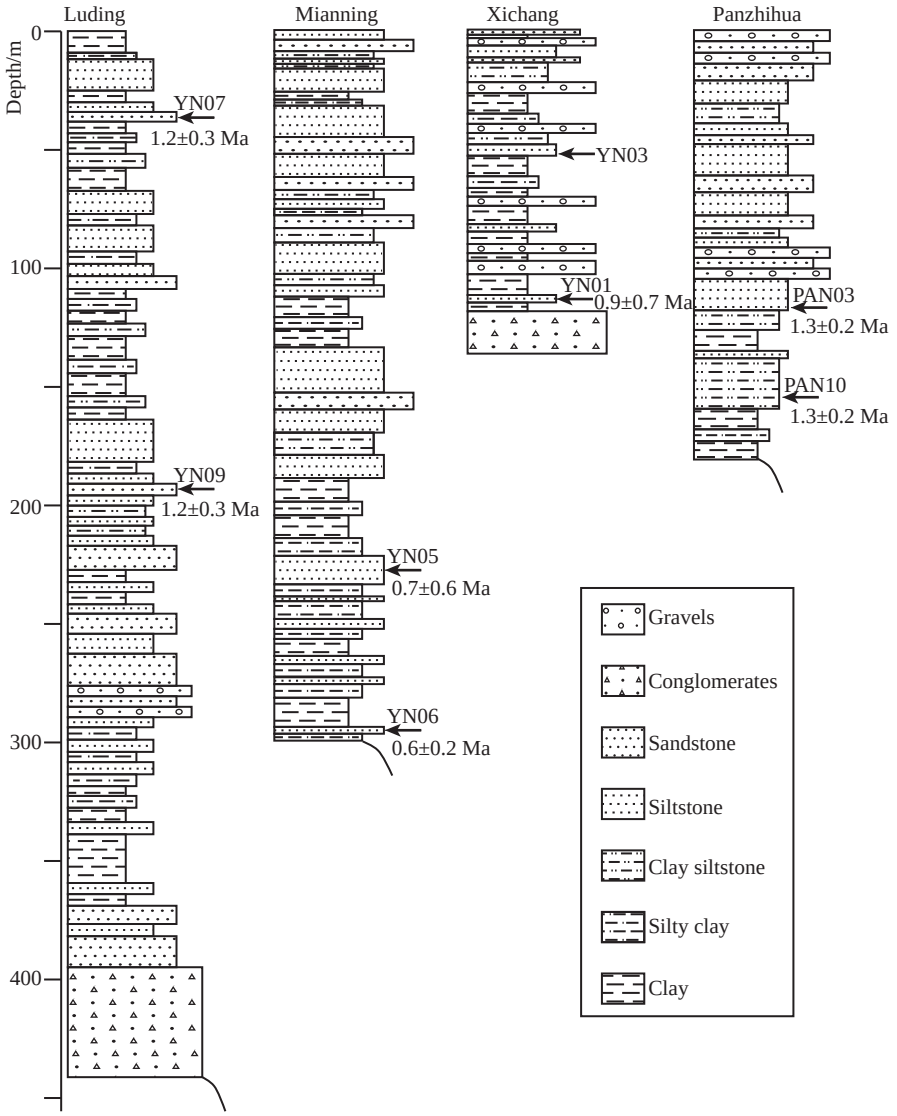

Fig. 3. Xigeda fluvial/lacustrine sediment sections along the Dadu and Anning Rivers showing lithologies and samples collected by this study. Locations of samples are marked with black arrows. The deposition ages are cited from Kong P et al. (2009) and Zheng Y et al. (2023).

trace element compositions were analyzed using an Agilent 7500a Q-ICP-MS at IGGCAS with analytical uncertainties of approximately 5% for elements with abundances $>10\times10^{-6}$ and 10% for those $<10\times10^{-6}$.

4. Results

Similar with sands collected from the modern Dadu River, the Xigeda samples are primarily composed of clinochlore (about 4%), muscovite (about 5%), quartz (>50%), anorthite (about 10%), and orthoclase (about 5%), indicating a granitoid affinity (Table 1). Compared with the bulk mineral compositions in most fluvial/lacustrine sediments, the Xigeda sediments have less kaolinite, illite, smectite, and other clay minerals, consistent with the previous results analyzed by Xu ZM et al. (2011), suggesting that weathering is generally limited for the Xigeda fluvial/lacustrine sediments. There are also several differences in the bulk mineral compositions among the various samples. The samples collected from the Xichang section contain the highest quartz percentage at 65%–70%, whereas those collected from the Panzhihua and Luding sections contain the lowest quartz content at only about 50%. Additionally, clay minerals are absent in the samples collected from the Xichang section, and orthoclase is absent in the Panzhihua section. These differences in the bulk mineral contents most likely reflect different weathering levels or influence from local material sources.

For the bulk major elements, the Xigeda lacustrine sediments are generally characterized by high SiO_2, with all samples >60%, and some of them >70%, indicating high compositional maturity, in general (Table 2). Most samples have low TiO_2 ($\leqslant$0.75%), P_2O_5 ($\leqslant$0.55%), and FeO* ($\leqslant$5%), and relatively high CaO (1.02%–8.51%), Na_2O (1.60%–2.52%) and K_2O (2.17%–2.71%), consistent with the compositions of the granitoid rocks distributed in the upper reaches of the Dadu River drainage (She ZB et al., 2006; de Sigoyer J et al., 2014). Compared with the sands of the present-day Dadu River, K_2O in the Xigeda sediments is higher than Na_2O, indicating an extensive secondary alteration after deposition. The K_2O/Na_2O ratios mainly range between 1.08 and 1.21, except for samples taken from the Panzhihua section containing higher ratios between 1.47 and 1.52, which represent a higher weathering level. The results show variable degrees of negative correlations for SiO_2 *vs.* FeO, MgO, MnO and CaO (Fig. 4), and a weak positive correlation for SiO_2 *vs.* Al_2O_3, reflecting an increasing mineralogical maturity with decreasing unstable components. The negative correlations of SiO_2 *vs.* MgO and CaO indicate that the carbonate in the clasts and matrix is primary (Feng R and Kerrich R, 1990). There is a positive correlation between SiO_2 and K_2O in this study due to the K metasomatism associated with weathering. A fair degree of scatter in SiO_2 *vs.* Na_2O and Fe_2O_3 can also arise from post-depositional weathering.

The Σ(rare earth element; REE) varies significantly among different samples, ranging from 113 μg/g to 223 μg/g and is lower than the 261 μg/g of the sands of the modern Dadu River (Table 2), owing to the different levels of mineralogical maturity and post-depositional modification of the Xigeda sediments. The chondrite-normalized patterns, especially the chondrite-Th-normalized patterns of REEs for both the Xigeda sediments and the sands of the modern Dadu River are consistent and are also consistent with the typical upper continental crust (Fig. 5), with LREE enrichment ($9.06\leqslant La_N/Yb_N\leqslant13.8$), flat HREE ($1.60\leqslant Gd_N/Yb_N\leqslant2.03$), and significant negative Eu-anomalies ($0.60\leqslant\delta Eu\leqslant0.81$). In general, the REEs show moderately fractionated patterns, with La_N/Yb_N ratios ranging between 9.06 and 13.8.

Similarly, both the normalized spidergrams by the North American shale and global upper continental crust for the Xigeda sediments and the sands of the modern Dadu River are similar (Fig. 5), implying a similar provenance. The abundances of V, Sc, Ni, Cr and Co greatly vary but, in general, are similar with the upper crustal and average shale values. The large-ion lithophile elements, Th and U, as well as Zr and Hf are relatively rich in the samples, indicating that weathering-resistant minerals, such as apatite and zircon, are relatively abundant. The lithophile dispersed elements, Sr, Nb, and Ba, are depleted, most likely owing to the extensive secondary alteration of feldspar in comparison with the global upper continental crust.

5. Discussions

5.1. An integrated north–south paleo-Dadu-Anning River

The chemical index of alteration (CIA) is commonly used to evaluate the weathering and alteration level of sediments from erosion, transportation, and sedimentation (Nesbitt HW and Young GM, 1989). The basic assumption is that during weathering, the percentage of inactive oxides (Al_2O_3) increases owing to the loss of active oxide (Na_2O, K_2O and

Table 1. Mineral compositions of the samples quantified based on X-ray diffractograms (%).

Sample	Sampling sections	Clinochlore	Muscovite	Quartz	Anorthite	Orthoclase	Calcite	Tremolite
YN01	Xichang	−	5	65	10	5	−	
YN03	Xichang	−	5	70	12	6	−	3
YN05	Mianning	4	7	64	8	6	3	4
YN06	Mianning	6	8	55	10	5	4	4
YN07	Luding	−	5	55	12	8	−	3
YN09	Luding	4	7	50	8	4	6	2
PAN03	Panzhihua	5	5	50	10	−	5	5
YN14	Modern Dadu river	3	5	50	18	7	−	5

Table 2. Major and trace element compositions of the Xigeda sediments.

Sample	YN01	YN03	YN05	YN06	YN07	YN09	YN14	PAN03	PAN10
Major elements/%									
SiO_2	72.5	76.4	65.6	65.0	73.1	61.7	69.6	69.4	74.2
TiO_2	0.72	0.68	0.63	0.63	0.55	0.64	0.52	0.67	0.66
Al_2O_3	12.3	11.3	10.7	11.1	12.3	10.9	13.7	11.5	11.6
Fe_2O_3	4.55	3.22	4.01	4.25	3.90	4.39	4.12	3.66	3.85
FeO	0.62	0.09	2.52	2.45	0.96	1.33	1.9	0.74	<0.20
MnO	0.06	0.04	0.07	0.07	0.05	0.14	0.08	0.12	0.06
MgO	1.18	0.67	1.94	1.97	1.10	1.69	1.48	1.57	1.18
CaO	1.28	1.02	6.59	6.61	1.68	8.51	2.95	3.62	1.09
Na_2O	2.03	2.09	1.98	1.96	2.52	1.80	3.48	1.59	1.60
K_2O	2.38	2.43	2.23	2.30	2.71	2.17	2.69	2.33	2.43
P_2O_5	0.52	0.28	0.36	0.37	0.32	0.35	0.29	0.13	0.14
LOI	3.04	2.46	5.76	6.15	2.21	8.01	1.20	4.04	2.64
Total	100.6	100.5	99.9	100.4	100.5	100.3	100.1	99.3	99.4
CIA	68.4	67.1	49.8	50.5	64.0	46.6	60.0	60.4	69.4
Trace elements/($\times10^{-6}$)									
Sc	10.5	8.14	9.34	9.85	8.55	9.88	9.87	11.8	10.0
Rb	108	102	94.6	96.2	111	94.7	99.0	96.9	95.1
Sr	150	157	252	252	192	210	274	145	119
Y	25.5	20.9	23.4	22.8	15.0	20.6	28.1	22.5	22.1
Zr	263	327	218	216	112	177	181	209	173
Nb	15.4	15.1	13.6	13.4	10.3	12.2	11.8	14.6	13.0
Cs	6.89	5.14	4.79	5.20	4.27	5.29	2.73	5.64	6.22
Ba	450	471	458	468	533	454	631	409	405
La	40.71	40.97	39.55	39.63	25.24	33.6	61.88	48.9	32.5
Ce	79.89	75.91	71.77	71.66	46.54	61.71	113.01	95.9	60.1
Pr	9.38	8.89	8.5	8.45	5.51	7.28	12.73	11.5	7.42
Nd	35.1	32.71	31.51	30.67	19.74	27.81	44.18	39.4	28.2
Sm	6.45	5.83	5.8	5.65	3.8	5.21	7.35	7.49	5.32
Eu	1.3	1.14	1.16	1.18	0.94	1.1	1.25	1.37	1.08
Gd	5.59	4.87	5.26	5.06	3.31	4.74	6.13	6.02	4.79
Tb	0.86	0.73	0.79	0.78	0.51	0.73	0.91	0.83	0.72
Dy	4.91	3.97	4.46	4.38	2.85	4.06	5.18	4.73	4.29
Ho	0.97	0.83	0.93	0.87	0.57	0.82	1.07	0.90	0.86
Er	2.65	2.32	2.55	2.45	1.55	2.26	3.07	2.44	2.41
Tm	0.41	0.35	0.39	0.37	0.24	0.34	0.48	0.36	0.37
Yb	2.67	2.29	2.48	2.43	1.5	2.24	3.22	2.40	2.42
Lu	0.41	0.35	0.38	0.37	0.23	0.34	0.5	0.37	0.38
Hf	7.64	9.31	6.48	6.20	3.23	5.19	5.42	6.06	5.01
Ta	1.30	1.31	1.21	1.18	0.85	1.01	1.12	1.16	1.06
Pb	20.9	17.3	18.7	19.2	18.7	22.3	18.8	18.6	20.0
Th	15.3	14.1	14.8	14.6	10.4	13.2	31.0	14.8	12.6
U	2.49	2.63	3.77	3.43	1.50	2.27	3.19	2.18	1.93
Cr	158	227	197	236	212	198	217	65.3	66.7
Ni	30.4	27.0	27.6	38.9	26.5	28.7	17.4	48.2	103
Cu	27.8	18.4	19.5	23.9	23.9	28.5	9.60	21.2	62.6
Zn	67.9	41.4	55.0	58.5	55.8	63.9	49.6	58.8	56.6
V	77.5	69.8	73.4	77.5	71.8	81.0	65.5	91.4	76.1
∑REE	191	181	176	174	113	152	261	223	151
La_N/Yb_N	10.3	12.1	10.8	11.1	11.4	10.2	13.1	13.8	9.06
La_N/Sm_N	3.94	4.39	4.26	4.38	4.15	4.02	5.26	4.08	3.81
Gd_N/Yb_N	1.69	1.72	1.72	1.69	1.78	1.71	1.54	2.03	1.60
δEu	0.66	0.65	0.64	0.67	0.81	0.67	0.57	0.60	0.64
δCe	0.99	0.96	0.95	0.95	0.95	0.95	0.97	0.98	0.94

CaO). Thus, the weathering degree is represented by the relative change between the percentages of Al_2O_3 and Na_2O+K_2O+CaO (Nesbitt HW and Young GM, 1989; Fedo CM et al., 1995). Compared with the CIA value of 60 for the sands of the modern Dadu River (Table 2), the Xigeda sediments in the Mianning section have a lower CIA value of

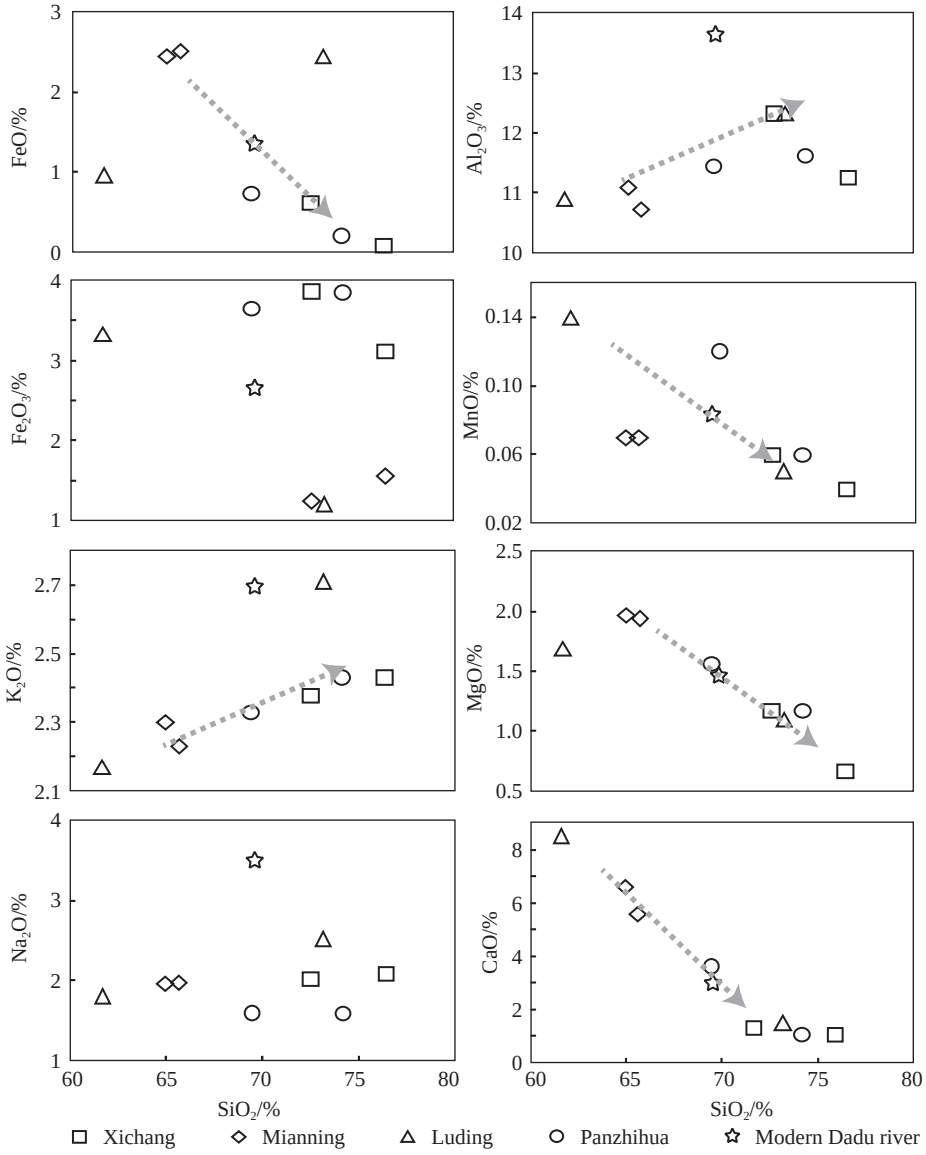

Fig. 4. Harker major element variation diagrams of the Xigeda sediments.

about 50, consistent with the average value of the unweathered upper crust (Taylor SR and Mclennan SM, 1985). The Xichang section has undergone the heaviest weathering, with the CIA values of 67–68. The CIA of the Luding section vary greatly as 47–64, and the CIA of the Panzhihua section (60–69) is similar with the sands taken from the modern Dadu River. The relatively lower CIA values (<70) are related to the source mainly consisting of granitoid rocks as well as limited weathering and alteration degree owing to the short after-deposition period.

The Xigeda samples exhibit an identical bulk compositional trend (Fig. 6), indicating a similar source rock assemblage and a similar erosion, transportation, and sedimentation environment. Therefore, the variation in the bulk compositions is derived from different weathering levels, in contrast to the viewpoint that the bulk composition varies owing to the different provenances (Xu ZM et al., 2011). The trend is slightly deviated from the theoretical line, indicating that the sediments have undergone K, Fe and Mg metasomatism with increased weathering (Fedo CM et al., 1995). In general, the weathering levels are not sufficiently high for the occurrence of incongruent dissolution of the potassic phases in the Xigeda sediments; hence, redirection toward the Al_2O_3 apex does not occur.

Therefore, consistent with the detrital zircon analysis results (Yang R et al., 2020; Zhao XD et al., 2021; Zheng Y et al., 2023), our analyses of bulk minerals, major and trace elements also indicate a shared provenance and an integrated paleo-river: (1) the bulk minerals for all Xigeda samples show a granitoid affinity (Table 2), corresponding to the Songpan-Ganzi flysch sediments and the widespread granitoid plutons upstream of the Dadu River; (2) the identical trends of the bulk major elements indicate similar initial compositions of source rocks (Fig. 6); and (3) both the normalized REE and trace elements show similar patterns (Fig. 5).

The A-CNK-FM and A-CN-K plots can be adopted to trace the source rocks under the basic principles that: (1) sediments derived from different source rocks will unlikely form an

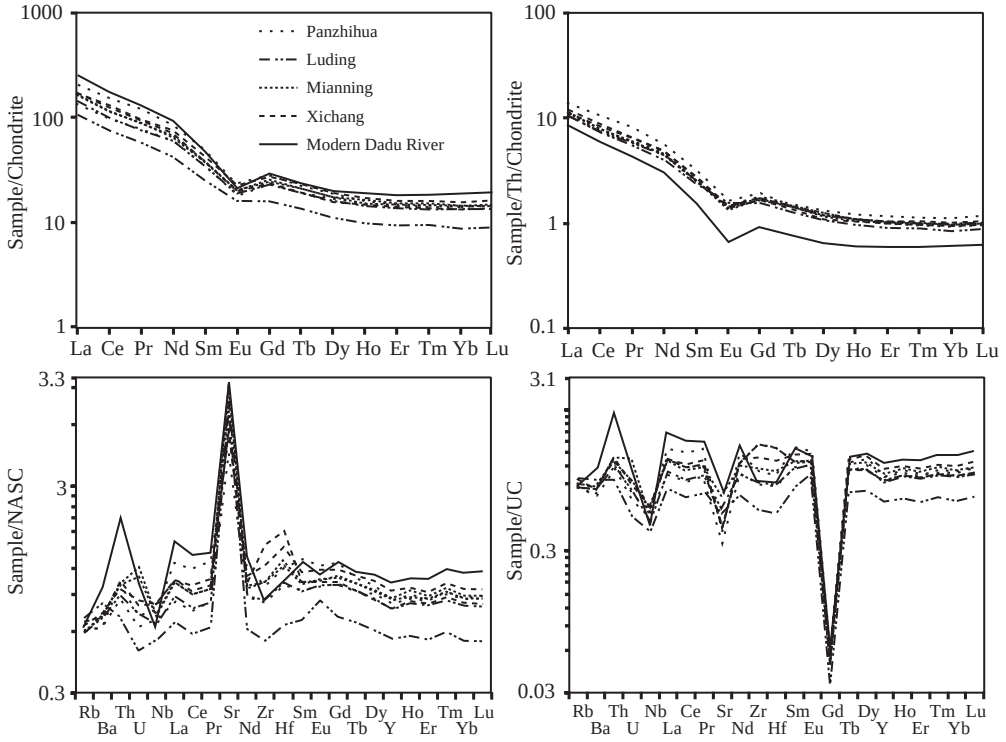

Fig. 5. Normalized REE and trace element diagrams for the Xigeda sediments.

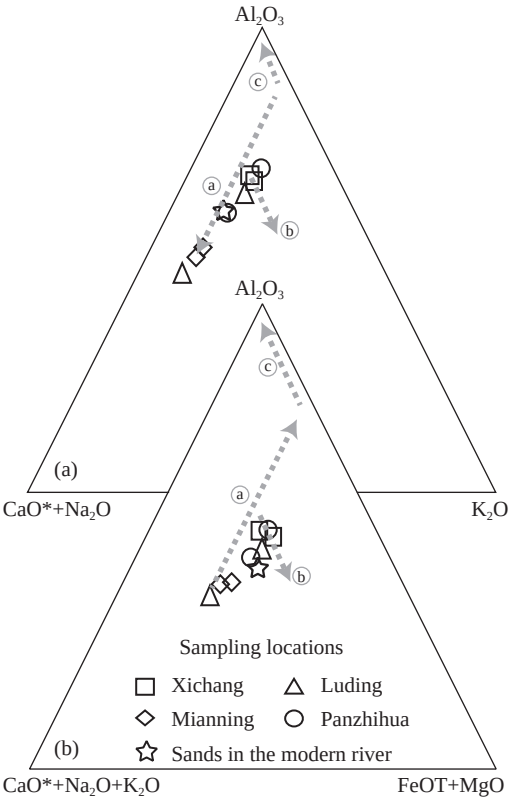

Fig. 6. Ternary plots of molecular proportions Al_2O_3-(Na_2O+CaO*)-K_2O and Al_2O_3-(CaO*+ Na_2O+K_2O) +(FeO_T+MgO) for the Xigeda sediments. The dashed arrow (a) shows the predicted weathering trend of the Xigeda sediments, and the nearly linear correlation suggests that different Xigeda sediments have similar initial material compositions; arrow (b) shows the additions of K or Fe and Mg to the weathered residues; and arrow (c) shows the predicted weathering trend once the residues contain little Na or About.

identical trends of both the bulk major and trace elements; (2) the lower intersection and the location of the linear trend along the CN-K and CNK-FM sides are closely related to the proportions between plagioclase and K-feldspar of the source rocks; (3) the slope of the linear trend is closely related to the weathering and alteration levels associated with erosion, transportation, and sedimentation of the source rocks (Nesbitt HW and Young GM, 1989; Fedo CM et al., 1995). Here in addition to the Xigeda samples, the available data for the main source rocks along the Dadu and Anning drainages are also compiled in the triangle plots (Fig. 7). The Xigeda samples are consistent with the field of the Songpan-Ganzi flysch in both the A-CN-K and A-CNK-FM plots, reflecting the major material contribution. Furthermore, they are also comparable with some values of the Songpan-Ganzi granites and Neoproterozoic complexes.

During sedimentary processes in water, trace elements Th, Co, Zr and Sc have low residence times and relatively low mobility; thus, they are suitable for provenance and tectonic setting discrimination (Taylor SR and Mclennan SM, 1985; Bhatia MR and Crook KAW, 1986; Gu XX et al., 2002). During primary weathering and transportation, these elements are transported quantitatively into clastic sediments; therefore, they are among the most reliable indicators of the parent materials. Both the Th-Sc-Zr/10 and Th-Co-Zr/10 plots show that the samples mainly fall in the field of the continental island arc. There is also a trend from the field of active continental margins to the field of the continental island arc likely due to weathering or sorting during transportation and sedimentation (Fig. 7). Therefore, the bulk trace elements of the Xigeda lacustrine sediments suggest that the tectonic settings of the source areas mainly consist of a continental

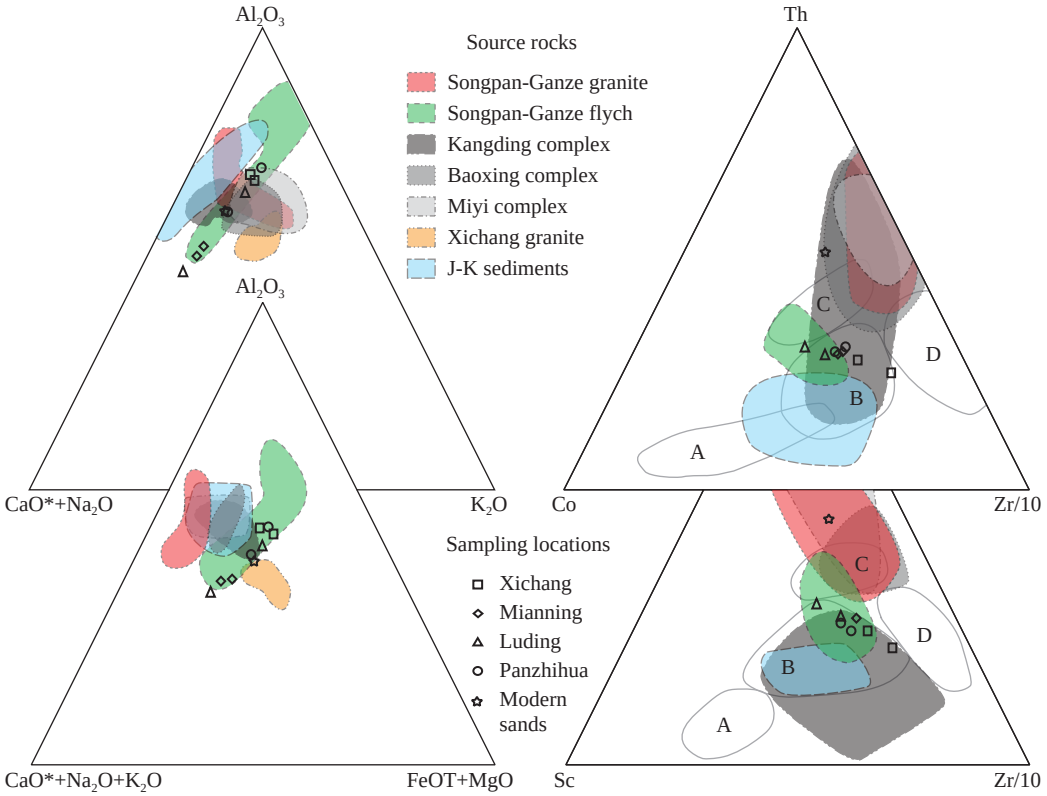

Fig. 7. A-CN-K, A-CNK-FM, Th-Co-Zr/10, and Th-Sc-Zr/10 plots of the Xigeda lacustrine/fluvial sediments for provenance and tectonic-setting discrimination. Dots represent the sediment samples taken from different sections. Dotted lines represent the dominant fields for their major source rocks (Data for Songpan-Ganzi grainites are from Zhao YJ et al., 2007; for Songpan-Ganzi flysch are from She ZB et al., 2006; for Kangding complex are from Li DP et al., 2009; for Miyi complex are from Guo CL et al., 2007; for Baoxing complex are from Liu SW et al., 2009; for J-K sediments are from Yang GC et al., 2010). Solid lines represent the dominant fields for the various tectonic settings (Bhatia MR and Crook KAW, 1986): A-Oceanic island arc; B-continental island arc; C-active continental margins; and D-passive margins.

island arc and active continental margin, corresponding to the western margin of the Yangtze Block and Songpan-Ganzi flysch belt, respectively (Xu ZQ, 1992; Xia Y et al., 2018). In addition, all Xigeda samples also fall in the fields for the source rocks of the Songpan-Ganzi flysch and Kangding complex (Fig. 7). Additionally, belonging to compatible and incompatible elements or belonging to heavy and light REE, the ratio of two immobile trace elements are considered as an useful tool to trace material provenance and the extent of sedimentary recycling during the formation of clastic rocks (Taylor SR and Mclennan SM, 1985). The Th/Co *vs.* La/Th, Th/Co *vs.* Zr/Co, La/Th *vs.* Hf, and Th/Co *vs.* La/Sc diagrams also suggest that the Songpan-Ganzi flysch and Kangding complex constitute the major sources of the Xigeda sediments (Fig. 8).

From the Luding section to the Panzhihua, Xichang, and Mianning sections, the samples gradually deviate from the fields for the source rocks of the Songpan-Ganzi flysch in the immobile element plots (Figs. 7, 8), especially the sands collected from the modern Dadu River, indicating a change of provenance between the paleo-Dadu-Anning River and the modern Dadu River. We attribute this discrepancy to the following possible reasons: (1) compared with the paleo-Dadu-Anning River, the modern Dadu River has lost its headwater stretching to the north of the Songpan-Ganzi flysch belt; (2) the material of the paleo-Xigeda lakes is mainly supplied by the paleo-Dadu-Anning River, but is also influenced by the local material source to a certain extent; (3) compared with the sediments in the modern Dadu River, the Xigeda sediments have experienced weathering and alteration after their deposition.

5.2. Cause of the capture of the paleo-Dadu River

The Xianshuihe fault splits into two major branches near the drainage divide—the Anninghe and Daliangshan faults (Fig. 9). Both faults are characterized by left-lateral slip with a dip-slip component (Wang E et al., 1998), complexly sharing an approximately 60 km left-lateral displacement to accommodate the movement of the Xianshuihe-Xiaojiang fault system. Therefore, the drainage divide is located at the transition/bending zone along a large strike-slip fault, where it is apt to form a local surface uplift owing to the transpressional stress fields. Such a transition/bending structure also triggered the September 5, 2022 Mw 6.8 Luding earthquake. With the regional surface uplift at the drainage divide associated with the continuous strike-slipping of the left-lateral Xianshuihe-Xiaojiang fault, the southward flow of the paleo-Dadu-Anning River was gradually blocked (Fig. 9) and was then captured and redirected toward the east near Shimian.

Based on the distribution of the Xigeda fluvial/lacustrine

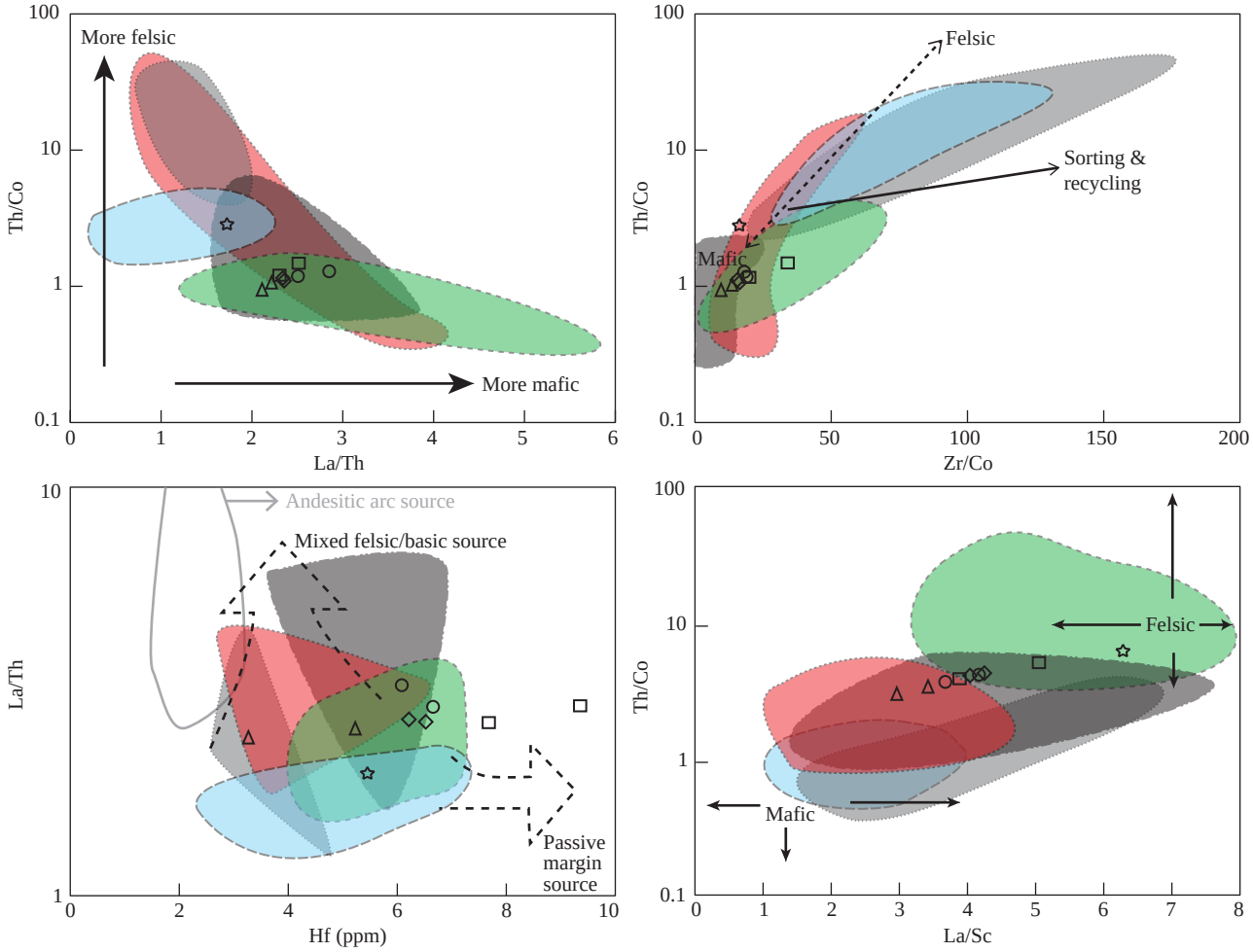

Fig. 8. Source rock discrimination diagrams for the Xigeda sediments on Th/Co *vs.* La/Th, Th/Co *vs.* Zr/Co, La/Th *vs.* Hf, and Th/Co *vs.* La/Sc.

sediments, Kong P et al. (2009) suggested the presence of a large paleo-lake stretching 110 km from north to south and 160 km from east to west. This lake was believed to have formed as a result of a large landslide blocking the middle Yangtze River. Deng B et al. (2020) argued existence of at least two large paleo-lakes at Panzhihua and Xichang. Although our results exhibit a similar material source for these fluvial/lacustrine sediments, the similar provenances are also consistent with the possibility that independent paleo-dammed lakes were filled with material carried by the integrated overflow paleo-Dadu-Anning River. The thickest section of the Xigeda lacustrine sediments is located at Luding, with a thickness of about 441 m, and thins out rapidly toward the south, indicating a heterogeneous distribution. In addition, landslide masses underneath the Xigeda lacustrine sediments have been identified on both sides of the modern Dadu River south of Luding County (Chen ZL et al., 2004). Therefore, the Xigeda sediments at Luding were most likely originated from a dammed lake associated with a paleo-landslide likely triggered by an earthquake. In contrast, the deep incised valley of the Anning River was considered as a result of the extension corresponding to the post-orogenic collapse of the eastern margin of the Tibetan Plateau (Wang E et al., 1998). This extension is characterized by normal-fault boundaries and resulted in the formation of the Anning graben (He HL et al., 2008). Therefore, the lacustrine sediments at Mianning and Xichang were most likely related to a paleo-dammed lake associated with a local depression.

Several models have been previously proposed to explain the geodynamics of the stream network reorganization that occurred in the southeastern Tibetan Plateau, including the lateral extrusion of the Chuandian Block along large crustal-shearing faults corresponding to the progressive convergence between the Indian and Eurasian plates (Tapponnier P et al., 2001), gravitational spreading of the elevated crustal material (Copley A, 2008), and dynamic channel flow within the lithosphere or asthenosphere (Clark MK and Royden LH, 2000; Shi XH et al., 2017). However, these driving forces are not mutually exclusive and probably result together in a regional river network rearrangement associated with locally focused uplift. Particularly in southeastern Tibet, the lateral rotation around the Eastern Himalayan syntaxis and the extrusion of the Chuandian Block probably driven by deep tectonic movement result in the formation of several large strike-slip fault systems, such as the Dali fault system, Xiaojiang fault system, and Xianshuihe fault system, which once conversely transected the elevated planation into locally focusing uplifts and depressions.

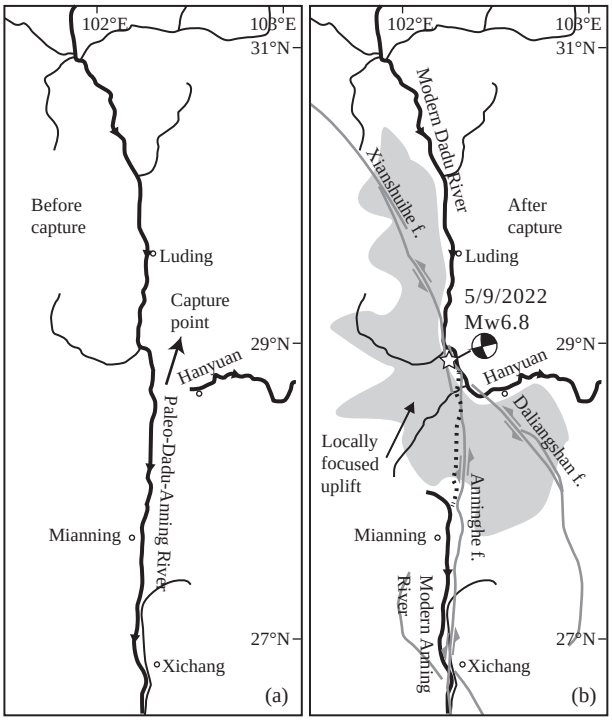

Fig. 9. Summary of captures for the paleo-Dadu-Anning River. a–Recovered paleo-Dadu River once flowed directly south into the palao-Anning River, constituting an about N–S connected paleo-Dadu-Anning River; b–after the suggested capture due to locally focused uplift, the paleo-Anning River was beheaded, and the Dadu River was redirected toward the east.

5.3. Timing of the River Rerouting

Paleomagnetic dating of the Xigeda Formation initially suggested a depositional age ranging between 3.29 Ma and 1.78 Ma (Qian F et al., 1984). Then, this method was widely applied in the dating of the Xigeda sediments in different locations, with results ranging from 4.3 Ma to 2.6 Ma (Luo YL and Liu DS 1998; Jiang FC et al., 1999; Wang SB et al., 2006; Yao HT et al., 2007). However, determining an absolute age was difficult, considering that most sections only record normal-polarity paleomagnetic signals. Given the large differences within the same strata, electron spin resonance (ESR) dating of the Xigeda Formation has only been used to test the paleomagnetic results so far (Yao HT et al., 2007; Wang P et al., 2011). Kong P et al. (2009) obtained 1.58–1.34 Ma for these fluvial/lacustrine sediments using cosmogenic nuclide burial dating, and thus, proposed a rearrangement of the middle Yangtze River during this period. Based on provenance and thermochronological studies, initial fluvial incision of the dammed lake and the formation of the modern river system were similarly inferred before the Early Pleistocene (Zhao XD et al., 2021). Based on low temperature thermochronology dating, Yang R et al. (2020) suggested the uplifting of the drainage divide between the Dadu and Anning rivers starting since around 2.0 Ma.

In recent years, cosmogenic nuclide burial dating has been considered as one of the few useful avenues to directly date lacustrine/fluvial sediments. The results showsigificant variations in depositional ages (Fig. 3) —1.2 Ma ago at Luding (Zheng Y et al., 2023), 1.6–1.3 Ma ago at Panzhihua (Kong P et al., 2009), 0.6–0.5 Ma ago at Mianning, and about 0.8 Ma ago at Xichang between Luding and Panzhihua (Zheng Y et al., 2023). Therefore, the presence of both the elevated drainage divide and oversteep gradients in the headstream of the modern Anning River suggest that the capture of the paleo-Dadu-Anning River near Shimian (Fig. 9) and the beheading the paleo-Anning River were a result of regional surface uplift occurring around 2.0 Ma (Yang R et al., 2020). This uplift was likely completed within the recent 0.6 Ma, as indicated by the deposition ages.

6. Conclusions

Fluvial/lacustrine sediments with thicknesses of hundreds of meters are widely distributed along the present-day Dadu and Anning drainages, representing the only sedimentary records of regional river network reorganization associated with the Late Cenozoic tectonic activities. Based on bulk mineral, major and trace analyses, the following conclusions were drawn:

(i) All Xigeda sediments in this study were derived from similar material sources mainly consisting of the Songpan-Ganzi flysch belt along the western margin of the Yangtze Block and upstream of the modern Dadu River. This suggests an about N–S integrated paleo-Dadu-Anning River once flowing through the present-day drainage divide and the occurrence of the river capture near Shimian County.

(ii) The rearrangement of the paleo-Dadu-Anning River appears to be closely related to the locally focused uplift driven by strong activities of the Xianshuihe-Xiaojiang fault system. The drainage divide is located at the transition/bending zone along the Xianshuihe-Xiaojiang strike-slip fault, where it is apt to form a local surface uplift owing to the transpressional stress fields.

(iii) The Xigeda sediments at Panzhihua, Xichang, Mianning, and Luding sections were deposited about 1.3 Ma ago, about 0.9 Ma ago, about 0.6 Ma ago, and about 1.2 Ma ago from south to north, respectively. Thus, the capture of the paleo-Dadu River resulted from the local surface uplift starting since about 2.0 Ma, which was likely completed within the recent 0.6 Ma.

CRediT authorship contribution statement

Yong Zheng and Hai-bing Li conceived of the present idea. Yong Zheng wrote and revised the paper with support from all authors and drew all the figures. Jia-wei Pan, Ping Wang, Ya Lai, and Zheng Gong participated in the field work. All authors discussed the results and contributed to the final manuscript.

Declaration of competing interest

The authors declare no conflicts of interest.

Acknowlegements

This work was financially supported by the Natural Science Foundation of China (41941016; 42072240; 41830217), Ministry of Science and Technology of China (2019QZKK0901, 2021FY100101), Key Special Project for Introduced Talents Team of the Southern Marine Science and Engineering Guangdong Laboratory (GML2019ZD0201), China Geological Survey (DD20221630), and Special Fund of the Institute of Geophysics, China Earthquake Administration (DQJB20B21).

References

Bai MK, Chevalier ML, Pan JW, Replumaz A, Leloup PH, Métois M, Li HB. 2018. Southeastward increase of the late Quaternary slip-rate of the Xianshuihe fault, eastern Tibet. Earth and Planetary Science Letters, 485, 19–31. doi: 10.1016/j.epsl.2017.12.045.

Bhatia MR, Crook KAW. 1986. Trace element characteristics of graywackes and tectonic setting discrimination of sedimentary basin. Contributions to Mineralogy and Petrology, 92, 181–193 . doi: 10.1007/BF00375292.

Chen ZL, Sun ZM, Royden LH, Zhang XY. 2004. Landslide blocked lake: Origin of the Xigeda formation in Luding, Sichuan and its significance. Quaternary Sciences, 24(6), 614–620 (in Chinese with English abstract).

Clark MK, Royden LH. 2000. Topographic ooze: Building the eastern margin of Tibet by lower crustal flow. Geology, 28(8), 703–706. doi: 10.1130/0091-7613(2000)28<703:TOBTEM>2.0.CO;2.

Clark MK, Schoenbohm LM, Royden LH, Whipple KX, Burchfiel BC, Zhang X, Tang W, Wang E, Chen L. 2004. Surface uplift, tectonics, and erosion of eastern Tibet from large-scale drainage patterns. Tectonics, 23, TC1006. doi: 10.1029/2002TC001402.

Copley A. 2008. Kinematics and dynamics of the southeastern margin of the Tibetan Plateau. Geophysical Journal International, 174(3), 1081–1100. doi: 10.1111/j.1365-246X.2008.03853.x.

de Sigoyer J, Vanderhaeghe O, Duchêne S, Billerot A. 2014. Generation and emplacement of Triassic granitoids within the Songpan-Ganze accretionary-orogenic wedge in a context of slab retreat accommodated by tear faulting, Eastern Tibetan plateau, China. Journal of Asian Earth Sciences, 88, 192–216. doi: 10.1016/j.jseaes.2014.01.010.

Deng B, Chew D, Mark C, Liu SG, Cogné N, Jiang L, Sullivan GO, Li ZW, Li JX. 2020. Late Cenozoic drainage reorgnization of the paleo-Yangtze river constrained by multi-proxy provenance analysis of the Paleo-lake Xigeda. Geological Society of American Bulletin, 133(1–2), 0–13. doi: 10.1130/B35579.1.

Fedo CM, Nesbitt HW, Young GM. 1995. Unraveling the effects of potassium metasomatism in sedimentary rocks and paleosols, with implications for paleoweathering conditions and provenance. Geology, 23(10), 921–924. doi: 10.1130/0091-7613(1995)023<0921:UTEOPM>2.3.CO;2.

Feng R, Kerrich R. 1990. Geochemistry of fine-grained clastic sediments in the Archean Abitibi greenstone belt, Canada: Implications for provenance and tectonic setting. Geochimca et Cosmochimca Acta, 54(4), 1061–1081. doi: 10.1016/0016-7037(90)90439-R.

Gu XX, Liu JM, Zheng MH, Tang JX, Qi L. 2002. Provenance and tectonic setting of the proterozoic turbidites in Hunan, South China: geochemical evidence. Journal of Sedimentary Research, 72(3), 393–407. doi: 10.1306/081601720393.

Guo CL, Wang DH, Chen YC, Zhao ZG, Wang YB, Fu XF, Fu DM. 2007. SHRIMP U-Pb zircon ages and major element, trace element and Nd-Sr isotope geochemical studies of a Neoproterozoic granitic complex in western Sichuan: Petrogenesis and tectonic significance. Acta Petrologica Sinica, 23(10), 2457–2470 (in Chinese with English abstract).

He HL, Oguchi T. 2008. Late Quaternary activity of the Zemuhe and Xiaojiang faults in southwest China from geomorphological mapping. Geomorphology, 96(1–2), 62–85. doi: 10.1016/j.geomorph.2007.07.009.

Jiang FC, Wu XH, Xiao GH. 1999. On the age of the Xigeda Formation in Luding, Sichuan, and its neotectonic significance. Acta Geologica Sinica, 73(1), 1–6 (in Chinese with English abstract). doi: 10.1111/j.1755-6724.1999.tb00806.x.

Kong P, Granger DE, Wu FY, Caffee MW, Wang YJ, Zhao XT, Zheng Y. 2009. Cosmogenic nuclide burial ages and provenance of the Xigeda paleo-lake: Implications for evolution of the Middle Yangtze River. Earth and Planetary Science Letters, 278(1–2), 131–141. doi: 10.1016/j.epsl.2008.12.003.

Li DP, Chen YL, Luo ZH, Zhao JX. 2009. Zircon SHRIMP U-Pb dating and Neoproterozoic metamorphism of Kangding and Yuanmou intrusive complexes, Sichuan and Yunnan. Journal of Earth Sciences, 20(6), 897–908. doi: 10.1007/s12583-009-0076-2.

Li ZX, Peter K, Zhou H. 2003. Geochronology of Neoproterozoic syn-rift magmatism in the Yangtze Craton, South China and correlations with other continents: evidence for a mantle superplume that broke up Rodinia. Precambrian Research. 122(1–4), 85–109. doi: 10.1016/S0301-9268(02)00208-5.

Liu SW, Yang K, Li QG, Wang ZQ, Yan QR. 2009. Petrogenesis of the Neoproterozoic Baoxing Complex and its constraint on the tectonic environment in western margin of Yangtze Craton. Earth Science Frontiers, 16(2), 107–118 (in Chinese with English abstract).

Luo YL, Liu DS. 1998. Cyclo-stratigraphy of the Xigeda Formation and the paleo-environmental implications. Quaternary Science, 18(4), 373–373 (in Chinese with English abstract).

Nesbitt HW, Young GM. 1989. Formation and diagenesis of weathering profiles. Journal of Geology, 97(2), 129–147 . doi: 10.2307/30065535.

Qian F, Xu SJ, Chen FB. 1984. Study on the paleomagnetism of the Xigeda Formation. Mountain Research, 2(4), 275–282 (in Chinese with English abstract).

Roger F, Malavieille J, Leloup PH, Xu ZQ. 2004. Timing of granite emplacement and cooling in the Songpan-Garzê Fold Belt (eastern Tibetan Plateau) with tectonic implications. Journal of Asian Earth Sciences, 22(5), 465–481. doi: 10.1016/S1367-9120(03)00089-0.

She ZB, Ma CQ, Mason R, Li JW, Wang GC, Lei YH. 2006. Provenance of the Triassic Songpan-Ganzi flysch, west China. Chemical Geology, 231(1–2), 159–175. doi: 10.1016/j.chemgeo.2006.01.001.

Shi XH, Wang Y, Sieh K, Weldon R, Feng LJ, Chan CH, Liu-Zeng J. 2017. Fault slip and GPS velocities across the Shan Plateau define a curved southwestward crustal motion around the eastern Himalayan syntaxis. Journal of Geophysical Research: Solid Earth, 123, 2502–2518. doi: 10.1002/2017JB015206.

Taylor SR, McLennan SM. 1985. The Continental Crust: Its Composition and Evolution. Oxford, Blackwell Scientific Publications.

Tapponnier P, Xu ZQ, Roger F, Meyer B, Arnaud N, Wittlinger G, Yang JS. 2001. Oblique stepwise rise and growth of the Tibet Plateau. Science, 294(5547), 1671–1677. doi: 10.1126/science.105978.

Wang E, Burchfiel BC, Royden, LH, Chen LZ, Chen JS, Li WX, Chen ZL. 1998. Late Cenozoic Xianshuihe/Xiaojiang and Red River fault systems of southwestern Sichuan and central Yunnan, China. Geological Society of America special paper, 327, 1–108 . doi: 10.1130/0-8137-2327-2.1.

Wang P, Li JP, Wang JC, Liu CR, Han F, Gao L. 2011. Quartz Ti-center in ESR dating of Xigeda formation in Sichuan and contrast with

magnetic stratigraphic profiles. Nuclear Techniques, 34(2), 111–115 (in Chinese with English abstract).

Wang SB, Zhao ZZ, Qiao YS, Jiang FC. 2006. Age and paleoenvironment of Xigeda Formation in Luding, Sichuan. Quaternary Sciences, 26(2), 257–264 (in Chinese with English abstract).

Xia Y, Xu XS, Niu YL, Liu L. 2018. Neoproterozoic amalgamation between Yangtze and Cathaysia blocks: The magmatism in various tectonic settings and continent-arc-continent collision. Precambrian Research, 309, 56–87. doi: 10.1016/j.precamres.2017.02.020.

Xu ZM, Liu WL, Huang RQ, Zhang GH. 2011. Material composition and provenance analysis for Xichang Xigeda Formation. Quaternary Sciences, 31(2), 378–396 (in Chinese with English abstract). doi: 10.3969/j.issn.1001-7410.2011.02.20.

Xu ZQ. 1992. The Orogenic Process of Songpan-Ganzi Orogenic Belt, China. Beijing, Geological Publishing House (in Chinese).

Yang GC, Yu BS, Chen JJ, Yao JM, Li SY, Wu YH. 2010. Geochemical research on rare earth elements of argillaceous rocks of Upper-Jurassic and Cretaceous in the Western Sichuan Foreland Basin. Geoscience, 24(1), 140–150 (in Chinese with English abstract).

Yang R, Suhail HA, Gourbet L, Willett SD, Fellin MG, Lin XB, Gong JF, Wei XC, Maden C, Jiao RH, Chen HL. 2020. Early Pleistocene drainage pattern changes in Eastern Tibet: Constraints from provenance analysis, thermochronometry, and numerical modeling. Earth and Planetary Science Letters, 531, 115955. doi: 10.1016/j.epsl.2019.115955.

Yao HT, Zhao ZZ, Qiao YS, Li CZ, Wang SB, Wang Y, Chen YS, Jiang FC. 2007. Magneto stratigraphic dating of the Xigeda formation in Mianning, Sichuan and its significance. Quaternary Science, 27(1), 74–84 (in Chinese with English abstract).

Zhao XD, Zhang HP, Tao YL, Wang Y, Pang JZ, Ma Y, Zhang JW, Ma ZF, Xiong JG. 2021. Pliocene to Early Pleistocene drainage reorganization in eastern Tibet inferred from detrital zircons. Geophysical Research Letters, 48, e2021GL094563 . doi: 10.1029/2021GL094563.

Zhao YJ. 2007. Mesozoic granitoids in eastern Songpan-Garzê: geochemistry, petrogenesis and tectonic implications. Guangzhou, University of Chinese Academy of Sciences, Ph. D thesis (in Chinese with English abstract).

Zheng Y, Li HB, Pan JW, Gong Z, Wang P, Lai Y, Zhao ZB, Liu FC. 2023. Mid-Pleistocene drainage rearrangement of the Dadu River in response to plate convergence in southeastern Tibet. Quaternary Research, 1–18. doi: 10.1017/qua.2022.71.